High-precision, gelatin-based, hybrid, bilayer scaffolds using melt electro-writing to repair cartilage injury

Yu Han [a,b,1], Bo Jia [c,1], Meifei Lian [b,d,1], Binbin Sun [a,b], Qiang Wu [a], Benlin Sun [a,b], Zhiguang Qiao [e,**], Kerong Dai [a,b,*]

[a] *Department of Orthopedic Surgery, Shanghai Key Laboratory of Orthopedic Implants, Shanghai Ninth People's Hospital, Shanghai Jiao Tong University School of Medicine, Shanghai, 200011, China*
[b] *Clinical and Translational Research Center for 3D Printing Technology, Shanghai Ninth People's Hospital, Shanghai Jiao Tong University School of Medicine, Shanghai, 200011, China*
[c] *Department of Orthopedics, Shanghai General Hospital, Shanghai Jiao Tong University School of Medicine, Shanghai, 200080, China*
[d] *Department of Prosthodontics, Shanghai Ninth People's Hospital, College of Stomatology, Shanghai Jiao Tong University School of Medicine, National Clinical Research Center for Oral Diseases, Shanghai Key Laboratory of Stomatology & Shanghai Research Institute of Stomatology, Shanghai, 200011, China*
[e] *Department of Orthopedic Surgery, Renji Hospital, South Campus, Shanghai Jiao Tong University School of Medicine, Shanghai, 201112, China*

A R T I C L E   I N F O

A B S T R A C T

Articular cartilage injury is a common disease in the field of orthopedics. Because cartilage has poor self-repairing ability, medical intervention is needed. Using melt electro-writing (MEW) technology, tissue engineering scaffolds with high porosity and high precision can be prepared. However, ordinary materials, especially natural polymer materials, are difficult to print. In this study, gelatin was mixed with poly (lactic-co-glycolic acid) to prepare high-concentration and high-viscosity printer ink, which had good printability and formability. A composite scaffold with full-layer TGF-β1 loading mixed with hydroxyapatite was prepared, and the scaffold was implanted at the cartilage injury site; microfracture surgery was conducted to induce the mesenchyme in the bone marrow. Quality stem cells thereby promoted the repair of damaged cartilage. In summary, this study developed a novel printing method, explored the molding conditions based on MEW printing ink, and constructed a bioactive cartilage repair scaffold. The scaffold can use autologous bone marrow mesenchymal stem cells and induce their differentiation to promote cartilage repair.

1. Introduction

Diseases, as well as cartilage injuries, such as osteoarthritis and traumatic arthritis, are common in orthopedics. Owing to the lack of blood vessels and nerves, cartilage has poor repairability. At present, few treatment methods, such as microfracture, autologous chondrocyte implantation, and joint replacement, are used clinically to repair these damages. However, these methods still have limitations in cartilage regeneration, such as poor repair effect and damage to the donor site. Biologically active scaffolds are a promising treatment method. An ideal tissue engineering scaffold should have good structure, suitable mechanical properties, appropriate degradation performance, and, most importantly, must promote cell adhesion, proliferation, and maintain the microenvironment to promote cell differentiation and gene expression [1–3].

In the past, the structure and composition of tissue-engineered scaffolds were relatively simple, mainly limited by the preparation process. The three-dimensional (3D) printing technology is a powerful tool for tissue engineering. It can allow the printing of different structures and components of scaffolds using various printing inks and controlling the printing path [4–6]. Melt electro-writing (MEW) is an integral part of 3D printing. By dissolving or melting the substance,

---

extruding the fiber, and then drawing it through an electrostatic field, thick fibers can be stretched and reduced in thickness, at the highest precision of 1 μm [7,8]. In the past, the study of the human articular cartilage revealed an issue that this cartilage is not uniform and has stratifications. Moreover, the surface and middle layers of cartilage tend to support structures and reduce joint friction; the deep layer is combined with the subchondral bone and plays a fixed role. This structure plays an important role in cartilage function [9–11]. Therefore, MEW can accurately simulate the multi-layer structure of normal cartilage, which is undoubtedly an advantage. In addition, different cartilage shapes can be prepared according to requirements [12,13].

In terms of materials, the most commonly used scaffolds for cartilage repair are natural or synthetic polymers, such as polysaccharides (chitosan, cellulose, starch, and pectin), polypeptides (gelatin and collagen), and polyesters (polylactic acid, polyglycolic acid, poly [lactic-co-glycolic] acid [PLGA], poly [3-hydroxybutyrate], and poly-ε-caprolactone). They are often used to improve the mechanical properties and biocompatibility of the scaffold [14–17]. As for MEW, due to higher requirements for printing and molding properties, PCL at this stage is still the main material. The degradation rate of PCL is slow, the biocompatibility is good, however, the biological activity is poor. Therefore, we need to study new materials for better repair of cartilage damage.

Gelatin is the product of partial collagen hydrolysis. It has various biologically active sequences and structural fragments that enhance cell functions and promote the formation of the extracellular matrix, including arginyl-glycine cell-binding sites and protease cleavage sites. It has good biocompatibility and biodegradability, is cost-effective, is easy to prepare, and has been widely used in the field of tissue engineering. However, gelatin has poor mechanical properties and can easily dissolve under physiological conditions; moreover, its printability is poor, particularly at room temperature [18–21].

PLGA is a copolymer approved by the Food and Drug Administration (FDA) for use in medicine and has excellent biodegradability and biocompatibility. By changing the ratio of lactic acid to glycolic acid in the copolymer, its degradation time can be altered. Moreover, PLGA is often used to prepare electrospun nanofibers for different applications, such as tissue engineering and the slow release of biologically active molecules, water purification, enzyme carriers, and sensors [22,23].

However, limited by technical capabilities, traditional electrospinning technology can only produce thin-layer, low-porosity, two-dimensional (2D) nanofiber membrane materials but cannot fabricate a 3D structure. Considering this, we took advantage of the high viscosity and the high concentration of gelatin/PLGA (G/P) hexafluoroisopropanol (HFIP) solution, the easy volatilization of the solvent, and the small diameter and large surface area of the electrospinning support. By slightly increasing the temperature of the printing substrate to accelerate solvent volatilization, the highly viscous solution can be rapidly shaped to print a 3D structure [24,25].

Transforming growth factor-β1 (TGF-β1) is a key regulator of cartilage differentiation of bone marrow mesenchymal stem cells (BMSCs). Often used as a key component of BMSCs into cartilage-inducing solution, it is considered to be the key to maintaining cartilage differentiation in vitro. TGF-β1 can also promote the synthesis of type II collagen in chondrocytes [26,27]. Hydroxyapatite (HA) can promote the hypertrophy of chondrocytes and the differentiation of chondrocytes into deep chondrocytes, and then promote the integration of repair cartilage and subchondral bone. Therefore, we install TGF-β1 in the full layer of the scaffold, and print HA mixed with G/P as the lower layer, to better promote the repair of cartilage damage [28].

In this study, we propose the use of a highly concentrated G/P solution to prepare a structural and functional biomimetic scaffold employing MEW technology. Given the characteristics of MEW technology, we prepared a high-precision natural biological material scaffold at room temperature for the first time. Natural material (gelatin) printing based on MEW was completed, and the characteristics of the

scaffold were verified. Related biological activities were also studied. The role of the scaffold in cartilage repair was further explored. Overall, G/P composite scaffolds are promising systems for supporting and promoting cartilage repair.

2. Materials and methods

2.1. Preparation and characterization of the scaffold

2.1.1. Preparation and characterization of gelatin/PLGA inks
We dissolved 1, 1.25, 1.5, and 1.75 g gelatin (240 g Bloom, Aladdin, China) in 10 mL HFIP to prepare 10, 12.5, 15, and 17.5% (w/v) gelatin solutions, respectively. Similarly, we dissolved 1, 1.25, 1.5, 1.75, and 2 g PLGA (molecular weight = 200,000, LA/GA = 85/15; Daigang, China) in 10 mL HFIP to prepare 5, 10, 12.5, 15, 17.5, and 20% (w/v) PLGA solutions, respectively. After testing the viscosity and printability, the G/P solution was prepared. The corresponding gelatin was first dissolved in 10 mL HFIP. Then, PLGA of corresponding concentration was added to prepare a G/P mixed solution. Precisely 0.3 g HA (diameter = 20 nm, Meilun, China) was added to 10 mL Gel/PLGA HFIP solution and mixed thoroughly using a magnetic stirrer to obtain the G/P/HA solution.

2.2. Rheological properties

Different rheological characteristics of gelatin, PLGA, G/P, and G/P/HA inks were investigated using a rheometer (Thermo HAAKE MARS 60, Germany). Viscosity was tested at 15–40 °C at a heating rate of 5 °C/min (frequency = 1 Hz). A 20-mm diameter rotor was used. At least three effective samples were tested for each ink sample.

2.2.1. Fourier transform infrared (FTIR) spectroscopy
FTIR spectroscopy (PerkinElmer Spectrum 100, USA) was used to characterize the chemical structure of gelatin, PLGA, and G/P. The infrared spectra of samples were measured at a wavelength range of 4000–500 cm^{-1}.

2.3. Preparation of microspheres

Microspheres were prepared using the double emulsification method. Precisely, 100 mL 0.1% (w/v) polyvinyl alcohol (PVA) solution was prepared, and 0.1 g of PLGA was dissolved in 1 mL dichloromethane (DCM). After cooling the PVA solution and PLGA/DCM solution in an ice bath, 500 μL of phosphate-buffered saline (PBS) was mixed with 1 mL of PLGA/DCM and dispersed by ultrasonic disintegrator. The resulting solution was added dropwise to the PVA solution using a micropump, stirred using a magnetic stirrer for 4 h, and centrifuged at 4000×*g* for 5 min. The supernatant was discarded, and the precipitate was washed with pure water. After repeating the washing and centrifugation steps three times, samples were freeze-dried.

To study the loading of TGF-β1 in PLGA microspheres, bovine serum albumin (BSA) was used as the analog protein. Briefly, 100 μg BSA was dissolved in 500 μL PBS, mixed with 1 mL PLGA/DCM solution, and then dispersed using an ultrasonic instrument. The remaining steps were the same as described above.

2.3.1. Determination of BSA/PLGA microsphere loading efficiency
After preparing microspheres with 100 mg PLGA according to the above method, these microspheres were freeze-dried and weighed. Precisely, 10 mg BSA/PLGA microspheres were dissolved in a solution of 0.9 mL 1 M NaOH and 0.1 mL PBS, stirred at 21 °C for 2 h, and then 1 mL 0.9 M HCl solution was added for neutralization. Using the BCA protein test kit (Biyuntian, Shanghai, China), a 20 μL sample was assessed for BSA determination. BSA loading efficiency (%) was determined as follows: The quantity of BSA (μg)/10 μg × 100 (%).

2.4. Preparation of multi-layer scaffolds

Using the MEW printer, the GP solution was placed in the barrel with a 23-gauge needle. The barrel temperature was set to 21 °C, and the printing panel was heated to 37 °C. Then, negative electric current was applied via the needle ground wire at an air pressure of 0.2 MPa. The printing panel was placed at a distance of 3 mm, and the voltage was set to −3 kV. After printing ten layers, the solution was changed to a cartridge containing cytokine microsphere ink. Exactly 10 mg of cytokine-containing microspheres was mixed with 10 mL pure water, and a 31-gauge needle was used. Air pressure and voltage were adjusted to 0.01 MPa and −2 kV, respectively, and the distance between the needle and the printing panel was 5 mm. Cytokine-containing microspheres were evenly sprayed on the scaffold using an Inkjet. After spraying, we switched to GP ink for printing and then printed alternately. The upper layer was GP (15% gelatin/15% PLGA), and the lower layer was GP/HA (15% gelatin/15% PLGA/3% HA). TGF-β1/PLGA microspheres were sprayed on all scaffolds. The upper and lower layers added up to 100 layers (each 1 mm). After printing, the scaffold was placed in a drying oven at 37 °C for 24 h.

2.4.1. In vitro protein release from BSA/PLGA microsphere-G/P composite scaffold

Briefly, 2 mL PBS (pH = 7.4) was added to the composite scaffold containing 10 mg microspheres, and the solution was placed in a shaker at 37 °C (100 rpm). At predefined time points, 1 mL of the solution was removed and replaced with 1 mL of fresh PBS, and the BSA content in the solution was measured using a BSA ELISA kit (Tongwei, China).

2.5. Scanning electron microscopy

Simple scaffolds (SS), microspheres, and microsphere-loaded composite scaffolds (CS) were imaged using a scanning electron microscope (S4800, Hitachi, Japan). The scaffold was placed on the scanning electron microscope objective table. Cross-sections of the scaffolds were frozen using liquid nitrogen and cut. All samples were sprayed with 6 nm platinum (OPC-80 T, SPI Supplies, USA) and observed.

2.6. Biomechanical examinations

The biomechanical properties of samples were tested using a biomechanical analyzer (Instron-5542, USA; n = 5 in each group). A 0.5 mm/min constant strain rate was used for all samples until 80% of maximum deformation was reached. Compression modulus and elasticity modulus were calculated according to the slope of the front stable section of the stress-strain curve [24].

2.7. Swelling and degradation

The swelling property of the scaffold was assessed using a gravimetric method. The initial dry weight (W0) of the constructs was noted, followed by their immersion in PBS (pH 7.4) at 37 °C. At predefined time points, the wet constructs were removed, the excess surface liquid was cleared using filter paper, and the swollen weight (Ws) was recorded. The study was conducted under identical conditions in triplicate, and the swelling ratio (SR) was determined using the following equation: SR (%) = (Ws – W0)/W0 × 100.

The degradation study was performed using PBS and lipase (Sigma-Aldrich, USA), as per a previously reported protocol [29]. Briefly, printed scaffolds were treated with PBS or 1% (w/v) lipase solution in PBS and maintained at 37 °C. Throughout the study (35 days), the enzyme solution was replaced every 3 days. Constructs immersed in PBS (without lipase treatment) were observed in parallel for their stability. Mass loss (ML) was calculated using the following formula: ML (%) = [(W0 – Wi)/W0] × 100 where W0 is the initial dry weight of the scaffold, and Wi is the final dry weight of the scaffold.

2.8. In vitro experiments

2.8.1. Cell isolation and culture

All animal treatments and experiments were approved by the Animal Care and Welfare Committee. Bone marrow mesenchymal stem cells (BMSCs) were collected from New Zealand rabbits (male, 2–4 weeks). The femurs and tibias of the rabbits were dissected, and both ends were cut. α-DMEM (Gibco, USA) (containing 10% fetal bovine serum, 1% penicillin-streptomycin, and 100 U/mL heparin sodium (HyClone, USA)) was repeatedly flushed into the medullary cavity. The washing solution was collected and centrifuged at $100 \times g$ for 5 min, the supernatant was discarded, and the cells were resuspended in media. The cells were seeded in a Petri dish and cultured at 5% CO_2 and 37 °C. The medium was changed after 2–3 days. The primary BMSCs were recorded as P0.

2.9. Cell seeding and culture on scaffolds

The scaffold was immersed in 75% ethanol for 2 h and washed with PBS three times for 5 min each. The scaffold was then placed in a 6-well plate. P2 BMSCs were collected via 0.25% trypsin digestion, pipetted, centrifuged, and resuspended. The cell concentration was adjusted to 5000 cells/mL, and 2 mL BMSCs suspension was added to each well. Cells were cultured in a 5% CO_2 incubator at 37 °C and the medium was changed every 2 days.

2.10. Cell adhesion and proliferation

The CCK-8 method was used to detect cell adhesion and proliferation on the scaffold. The scaffold was placed in a 96-well plate, the concentration of BMSCs was adjusted to 10,000 cells/mL using the abovementioned method, and 200 μL of cells were added to each well. On days 4, 7, 14, and 21, the cell scaffold was transferred to a clean 96-well plate. To this, 200 μL of medium with 10% CCK-8 reagent was added, and the plate was incubated for 1 h; then, 100 μL of the medium was moved to another clean 96-well plate and absorbance was measured using a microplate reader (Thermo Fisher Scientific, USA) at 450 nm (630 nm was used as a reference).

On days 4, 7, and 14, the cell-carrying scaffold was fixed with 4% paraformaldehyde and incubated with TRITC-phalloidine (Maokang, China. 1:200) at 21 °C for 45 min then with DAPI (Maokang, 1:1000) at 21 °C for 10 min, and observed using a fluorescence microscope (LEICA, Germany).

2.10.1. RNA isolation and quantitative reverse-transcriptase polymerase chain reaction (qRT-PCR)

To clarify the effect of each component of the scaffold, we used the relatively inert polymer material PCL, which is commonly used in MEW technology, as the scaffold substrate for the BMSCs (blank control), pure TGF-β and HA/TGF-β groups. The Direct-zol® RNA MiniPrep kit (Zymo Research, USA) was used to extract RNA from each group (n = 5 per group) according to the manufacturer's instructions. The qScriptTM cDNA synthesis kit (Quanta Biosciences, USA) and MiniOpticon real-time PCR detection system (BioRad, USA) was used to reverse transcription of the extracted mRNA to obtain cDNA, all the operations were performed following the manufacturer's instructions. SYBR Green FastMix kit (Quanta Biosciences, USA) and ABI 7300 real-time PCR system (Thermo Fisher, USA) were used to analyze gene expression. The expression of proteoglycan 4 (prg4), collagen II (col II), collagen X (col x), aggrecan (agc) and transcription factor Sox-9 (sox9) are standardized as β-actin (actb) expression and calculated using the $2^{-\Delta\Delta Ct}$ method. Supplementary Table 1 listed the primer sequences of prg4, col II, col x, sox9, agc and actb.

2.11. Immunofluorescence staining

After 21 days, the cell-carrying scaffold was fixed with 4% paraformaldehyde, soaked in Triton-X (0.1%) for 5 min, and washed with PBS three times for 5 min each. To clarify the effect of each component of the scaffold, we used the relatively inert polymer material PCL, which is commonly used in MEW technology, as the scaffold substrate for the blank control and pure TGF-β groups. It was then blocked with BSA solution at room temperature for 1 h, the excess liquid was aspirated, and the scaffold was incubated with corresponding primary antibodies (anti-AGC, anti-Collagen II, anti-Collagen X, and anti-SOX-9) (1:100, Abcam, UK) at 4 °C overnight. The scaffold was then washed with PBS three times for 5 min each. The scaffold was incubated with secondary antibody (1:500, Abcam, UK) at room temperature for 1 h, washed with PBS, incubated with FITC-phalloidine (1:200, MaoKang) at 21 °C for 2 h and with DAPI (1:1000, MaoKang) for 30 min at 21 °C. After washing with PBS three times for 5 min each, the samples were observed using a confocal microscope (LEICA, Germany). ImageJ was used to analyze the resulting images.

2.12. In vivo experiments

2.12.1. Surgical procedure

All animal operations and experiments were approved by the Animal Care and Welfare Committee. The in vivo experiments were conducted in three groups: blank, PLGA microsphere, and CS groups. Six-month-old male New Zealand rabbits weighing about 3–4 kg were reared at 27 °C under a 12-h light/dark cycle with a humidity of 55–65%. The animals were anesthetized with 50 mg/kg ketamine and 50 mg/kg xylazine. After anesthesia, a midline incision of the right knee was made, and the medial collateral ligament was cut from the inside of the patella to enter the joint cavity. A 4-mm wide and 2-mm deep defect was made between the condyles, and a 1-mm Kirschner wire was drilled through the subchondral bone to communicate with the marrow cavity. The damaged area was filled with each group of repair scaffolds, which divided into three groups (1, blank control (BC), no repair scaffold is added; 2, simple scaffold (SS), a scaffold formed solely by G/P printing, without HA and TGF-β microspheres; 3, CS, the lower layer was printed by G/P/HA, the upper layer was printed by G/P, and the full layer is loaded with TGF-β microspheres). Routine stitching was performed in the repair bracket. The animals were sacrificed at 3, 6, 12, and 24 weeks after surgery (n = 4).

2.12.2. Histology and immunofluorescence staining

Samples were collected at 3, 6, 12, and 24 weeks after surgery. The samples were routinely decalcified and embedded in paraffin. 10 times volume of EDTA decalcification solution was used to soak the samples, 21 °C, decalcification for 60 days, replace fresh decalcification solution every week. Standard hematoxylin and eosin (H&E; Thermo Scientific, USA) staining was used to assess cell distribution and tissue conditions. Anti-COL II, anti-COL I, anti-AGC, and anti-SOX9 primary antibodies (1:100, Abcam) were used for histochemical staining overnight at 4 °C, and corresponding biotin anti-mouse IgG secondary antibody was performed for 2 h in the dark at 21 °C. Then, SABC and DAB color reagents were added in turn. A light microscope (LEICA, Germany) was used to observe and evaluate the samples.

2.12.3. Biomechanical and biochemical evaluations

The sample compression modulus was measured according to the aforementioned method in section 2.1.9. After the mechanical test was completed, the sample was analyzed for collagen composition. Total collagen content was quantified using a hydroxyproline assay and type II collagen content was quantified using a sandwich enzyme-linked immunosorbent assay according to previously published methods [30, 31].

2.13. Statistical analysis

SPSS 25.0 statistical software (SPSS, USA) was used for data analysis. Quantitative data were expressed as the mean ± standard deviation. Independent sample t-tests and one-way analysis of variance were used to analyze the data. Results with P < 0.05 were considered statistically significant.

3. Results

3.1. Preparation of the CS

3.1.1. Preparation of bio-inks

As shown in Fig. 1A, the printed structure of the low-viscosity ink was more likely to collapse, whereas that of the high-viscosity ink could better maintain shape. FTIR was used to detect gelatin, PLGA, and their mixtures. Gelatin spectra showed peaks at 1194 and 1648 cm^{-1}, corresponding to amido III and amido I bonds, respectively. PLGA showed C–O and C=O at 1095 and 1756 cm^{-1}, which were also detected in the mixture. Considering that the properties of gelatin and PLGA in the mixture were stable, no new bond was formed, and the relative stability could be maintained. In contrast, we tested the rheological behavior of high-concentration gelatin, PLGA, and mixed HFIP solutions at different temperatures (Fig. 1C–E). The results showed that at a certain temperature, the volatilization speed of HFIP accelerated, which increased the viscosity of the ink from the liquid state with a certain flow. Fig. 1F and Figure.S1 shows the performance of the above three solutions under slightly tilted and upright positions to obtain an approximate idea of their viscosity. In addition, we tested the printing moldability of HFIP solutions of gelatin and PLGA at different ratios. Fig. 1G shows printing and molding effects. We aimed to print a high-precision natural polymer scaffold using 15% gel/15% PLGA and 12.5% gel/17.5% PLGA; therefore, we chose higher natural polymer ingredients at 15% gel/15% PLGA for follow-up experiments.

3.1.2. Fabrication of a simpler scaffold

Fig. 2A shows a schematic diagram of the printer in which the printing cylinder was maintained at 21 °C and the stage at 37 °C, thereby enhancing the volatilization of the solvent and improving the molding effect. Fig. 2B shows a schematic diagram of the printing model. The picture of stacked G/P (C1, C2) and G/P/HA (C3, C4) with 10 and 100 layers is shown in Fig. 2C. The morphology of the scaffold printed by G/P and G/P/HA as observed under the electron microscope is shown in Fig. 2D and E. The pore size of the scaffold was 400 μm. The morphology of the scaffold showed that after freeze-drying, the general structure remained good, but the surface of the fiber was altered. The vacuum environment might have caused the solvent to volatilize further, reducing the possible impact of the solvent.

The mechanical performance of the scaffold under compression and tension is shown in Fig. 2F–H. The presence of HA reduced a part of the elastic modulus of the scaffold, but it had no major influence on the compression modulus. Overall, the scaffold had good mechanical properties.

3.1.3. Preparation of microspheres

Fig. 3A shows the preparation of microspheres. We used the double emulsion method, and the microspheres generally performed well. Fig. 3B shows the basic morphology of the microspheres. It was observed that the size of the microspheres was relatively uniform, with a diameter of approximately 5 μm. Microspheres with a particle size of 3–4 and 2–5 μm accounted for 34.5 and 81.4%, respectively, of all microspheres, which met the needs of the users (Fig. 3C). We also used BSA as a standard for protein content detection, and the results showed that every 10 mg of microspheres contained 7.125 ± 1.102 μg of BSA. We prepared the microspheres in a suspension at a concentration of 1 mg/mL and measured the relationship between the flow rate and the quality of
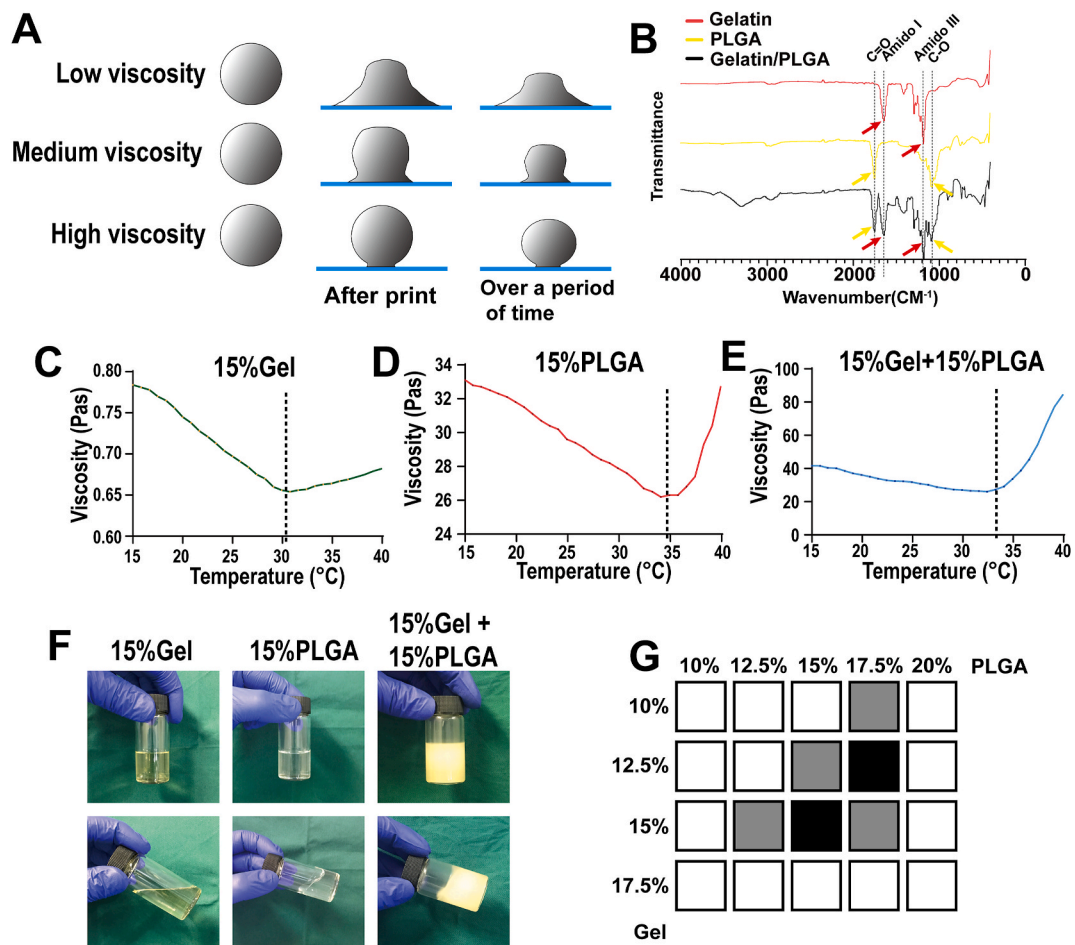
Fig. 1. Preparation of bio-inks. A) Schematic diagram of MEW electrospinning with different viscosities. B) FTIR spectroscopy results of gelatin, PLGA, and their mixtures. C–E) Rheological test results. F) Gross view dissolution performance. G) Printability and moldability (white represents printing difficulty or poor molding effect, gray represents ineffective printing, black represents relatively good printing). MEW, melt electro-writing; FTIR, Fourier transform infrared; PLGA, poly (lactic-co-glycolic acid).

microspheres (Fig. 3D and E). We sprayed 100 µg microspheres after every 10 layers of the printed scaffold.

3.1.4. Fabrication and testing of CSs

In the preparation process of the CS, we used MEW and Inkjet alternate printing. Inkjet 100 µg cytokine-carrying microspheres were sprayed every 10 layers of the printed scaffold so that the scaffold provided a better composite. Fig. 3G shows G/P and G/P/HA scaffolds loaded with microspheres and the specific morphology and structure of scaffolds. After compounding the microspheres, they were attached to the scaffold surface and maintained a certain degree of stability. Fig. 4A shows a schematic diagram of our scaffold design. The base material of the overall scaffold contained G/P and G/P/HA. The Inkjet was used to load TGF-β-loaded PLGA microspheres. In the lower layer, 3% HA was mixed to enable better bonding with the subchondral bone. The swelling of the scaffold and release of BSA were tested. The scaffold was in good condition in a liquid environment and could load and release protein normally. The degradation of the scaffold was measured in PBS- and enzyme-containing environments. In the enzyme-containing environment, the scaffold degraded quickly and could not maintain its shape for 2 weeks. In the PBS-containing environment, it could maintain its normal shape after 5 weeks, with approximately 90% of the mass intact. The degradation rate was similar to the cartilage regeneration rate [15, 32].

3.2. In vitro experiments

3.2.1. BMSCs adhesion and proliferation on the scaffold

To further understand the biocompatibility of the scaffold as well as the adhesion and proliferation of cells on the scaffold, we used BMSCs. After 4 days, the seeded cells were firmly attached to the scaffold (Fig. 4 E, F). After 7 days, the number of cells increased significantly, and by day 14, cells had covered the entire scaffold. Cell activity on the scaffold was good, and there were no evident dead cells, as shown in Fig. 4E. DAPI and F-actin staining revealed normal cell morphology (Fig. 4F). In addition, there were no apparent differences in adhesion and proliferation between the groups. Further verification using the CCK-8 test showed that the cell activity on the scaffolds was good in each group, and increased with time. After 21 days, the increase slowed, considering that the cells were in contact with each other; moreover, contact inhibition was noted (Fig. 4G and H). These results were consistent with the results of fluorescent staining, which showed good adhesion and proliferation on all scaffolds.

3.2.2. Cytokine-loaded microspheres induce chondrogenic differentiation and expression of specific proteins in various layers of the CS

BMSCs were seeded on the CS, and relative protein expression was observed after 21 days of culture and differentiation. Immunofluorescence staining, confocal microscopy, and qRT-PCR were used to detect relative protein levels and mRNA expression. To clarify the effect of each component of the scaffold, we used the relatively inert polymer material
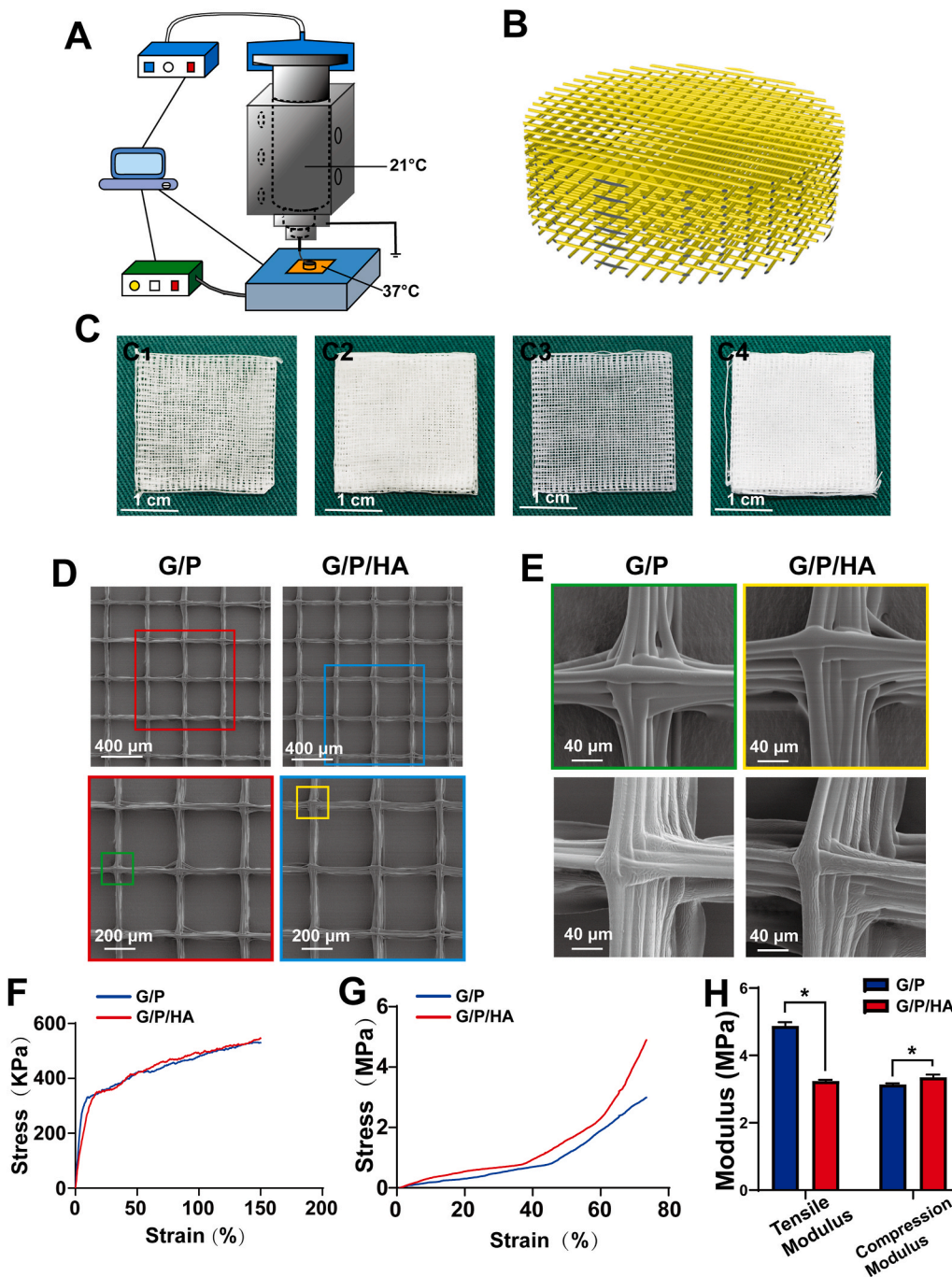
Fig. 2. Fabrication of simple G/P and G/P/HA MEW scaffolds. A and B) Schematic diagram of MEW and simple scaffold. C) Gross view of the simple G/P (C1, C2) and G/P/HA scaffold (C3, C4) (C1, C3: 10 layers; C2, C4:100 layers). D and E) Scanning electron microscopy images of G/P and G/P/HA scaffolds. F–G) Test curve of mechanical properties. H) Tensile and compression modulus. (*P < 0.05 compared with other groups) MEW, melt electrowriting; G/P, gelatin/PLGA; HA, hydroxyapatite.

PCL, commonly used in MEW technology, as the scaffold substrate for the BC and the pure TGF-β groups.

After cytokine induction, BMSCs differentiated into chondrocytes and expressed corresponding proteins (Fig. 5A). Sox9, as a marker protein of chondrocytes, was highly expressed in the three TGF-β groups but not in the G/P or G/P/HA scaffold groups. In contrast, G/P significantly promoted the expression of col II, and the presence of HA promoted the expression of col X. In addition, compared with pure TGF-β, PLGA/gelatin bioactive scaffold promoted high expression of agc. These results showed that the scaffold design based on gelatin had good feasibility for cartilage repair. The results of qRT-PCR verified that compared with TGF-β alone, PLGA/gelatin increased the expression of col II, agc, and sox9, whereas HA promoted the expression of col X. In addition, gelatin and PLGA increased the expression of prg4 and thus

promoted better cartilage repair.

3.3. In vivo cartilage injury repair following implantation of CSs

We used a rabbit femoral intercondylar cartilage injury model (Fig. 6A) to evaluate cartilage damage repair at 3, 6, 12, and 24 weeks after transplantation of various stents. Cartilage repair was completed at 12 weeks. To observe the subsequent cartilage repair further, the observation was extended to 24 weeks. Fig. 6B shows an image of a simple scaffold and CS labeled with pigment. A trephine was used to drill a circular cartilage injury with a diameter of 4 mm between the femoral and femoral condyles of a rabbit. We used a 1-mm Kirschner wire to penetrate the subchondral bone, then introduced bone marrow blood and filled the scaffold (Fig. 6C). We then observed the repair of cartilage
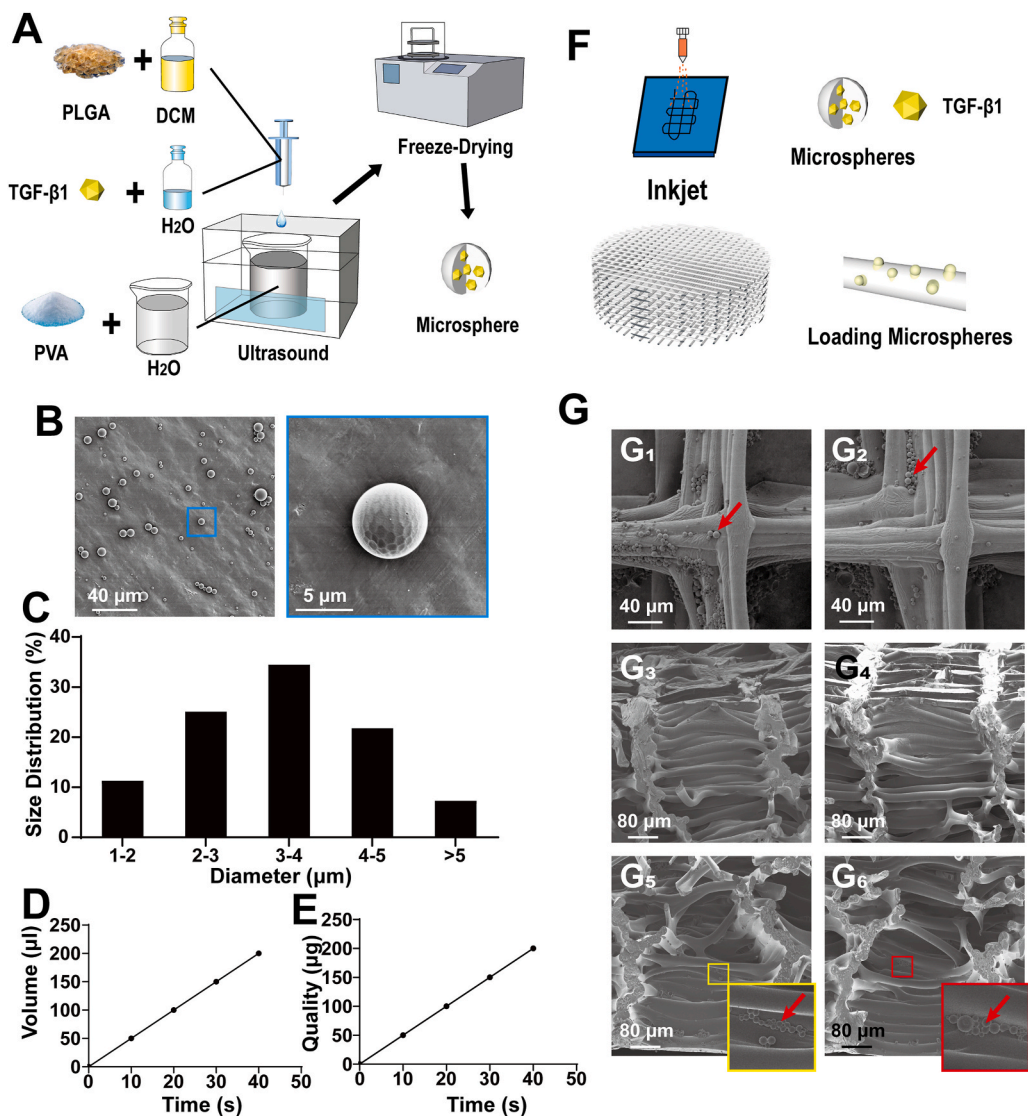
Fig. 3. Composite scaffold fabrication via alternate printing with MEW and Inkjet. A) Schematic diagram of the double emulsification method for microsphere production. B) Morphology of microspheres determined using scanning electron microscopy (SEM). C) Statistics of microsphere diameter distribution. D and E) Relationship of spray time and volume with the quality of Inkjet microspheres. F) Schematic diagram of Inkjet fabrication. G) Front and cross-section SEM images of microspheres adhered to the G/P scaffold (G1, G5), and G/P/HA scaffold (G2, G6); comparison of a cross-section SEM image of a simple G/P and G/P/HA scaffold (G3, G4). MEW, melt electrowriting; G/P, gelatin/PLGA; HA, hydroxyapatite.

damage after obtaining samples at fixed time intervals. The BC group showed poor damage repair after 3 and 6 weeks, and apparent scar tissue was noted. This damage partially healed after 12 weeks but was not completely healed after 24 weeks.

In the two experimental groups, although the damage was replaced by new cartilage after 6 and 12 weeks, the surrounding tissues had clear boundaries, especially after 6 weeks, and the boundary of the damage was observed in the cross-section. The dividing line between the scaffold and the surrounding tissues was significantly improved compared to 3 weeks. After 24 weeks, the damage in the BC group was still not repaired. In the simple scaffold group, new cartilage was formed in the damaged area, while in the CS group, new cartilage was observed to cover the damaged area and was relatively intact with the surrounding tissues. The cross-section also showed that the scaffold and the surrounding tissues were well-integrated (Fig. 6D).

To further evaluate cartilage healing, the injured area was incised and stained with H&E (Fig. 7, Figure S2). Similar to the overall observation, the BC group had some cartilage-like tissue formation at 24 weeks, but it was mainly scar tissue, and the tissue structure was heterogenous. This showed that 4-mm damage was difficult to repair. In contrast, because the scaffold provided good support to the cells, the new tissue structure was stable, showing a layered morphology, similar to that observed in the two scaffold groups after 3 and 6 weeks. This

morphology provided good support for subsequent cartilage tissue formation. In addition, the scaffold contained gelatin, which had good biocompatibility, and the regenerated tissue covered the injured area relatively completely. In the CS group, owing to the presence of bioactive factors, such as cytokines and HA, cartilage repair was further promoted. After 12 and 24 weeks, cartilage tissue with normal structure and shape was observed at the injured site.

In addition, because of the degradability of PLGA and gelatin, the degradation speed was more compatible with cartilage repair speed. After 12 weeks, the scaffold was mostly degraded, and only a small amount of scaffold residue was observed. The morphology of the repaired tissue was also confirmed by Sirius Red staining (Figure S3), which indicated that the collagen morphology of the CS after 12 and 24 weeks was good. Therefore, adding cytokine-loaded microspheres helped enhance the biological activity of the scaffold significantly.

Twenty-four weeks after injury and scaffold implantation, immunohistochemical analysis of cartilage tissue was also performed to evaluate the expression of col II, col I, prg4, and sox9. In the CS group, we observed that col II had a higher expression level and col I showed relatively lower expression. Moreover, prg4 expression on the scaffold surface was closer to that on normal cartilage, and the surface of the regenerated cartilage was smoother with good wear resistance. Besides, sox9 expression was close to that in normal cartilage.
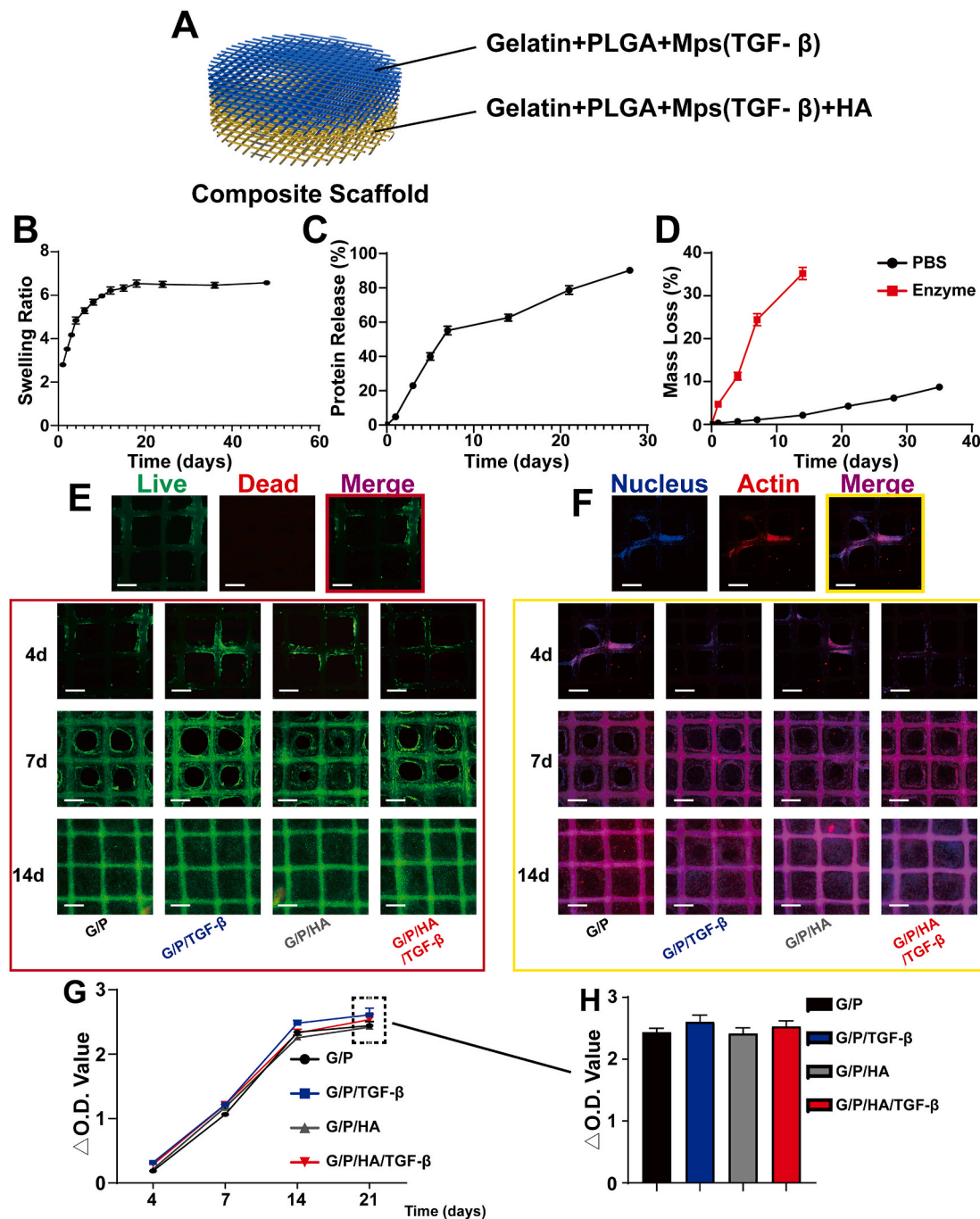
Fig. 4. BMSCs adhesion and proliferation on the scaffolds. A) Schematic diagram of the composite scaffold design. B, C and D) Swilling, protein release, and degradation curve of the composite scaffold. E and F) BMSCs adhesion and proliferation on scaffolds on days 4, 7, and 14. E) Live and dead cells. F) n-nucleus and F-actin staining. (The first row shows the schematic diagram of E: Live, dead and live/dead merged, F: nucleus, actin and nucleus/actin merged). G and H) CCK-8 assay results at various time points. (Scale Bar: 200 μm) (*P < 0.05 compared with other groups). BMSCs, bone marrow mesenchymal stem cells.

Overall, the protein expression in the CS group was more similar to that in the normal cartilage group. Moreover, the stent-only group had a more obvious cartilage repair effect than the control group. After the repaired cartilage was removed using a ring drill, mechanical and component analyses were performed to analyze the content of total collagen and col II. The results showed that after 3 weeks, the implanted scaffold showed increased production of total collagen and col II. After 24 weeks, the total collagen content was stable and higher than that in the BC group. The CS group had a higher col II content, which showed that the CS had a better effect of promoting cartilage repair. In addition, the compression modulus test showed that the composite stent group had better mechanical properties (Fig. 8 and Figure.S4).

4. Discussion

In this study, we designed and developed a new type of G/P MEW scaffold loaded with TGF-β1 microspheres and HA, which are the key growth factors for cartilage induction and differentiation [33,34]. In the field of biomedical engineering, to better repair cartilage damage, several studies are in progress to develop a good 3D structure and increase biocompatibility. This will enable stem cells to not only adhere and proliferate but also maintain a microenvironment for cartilage
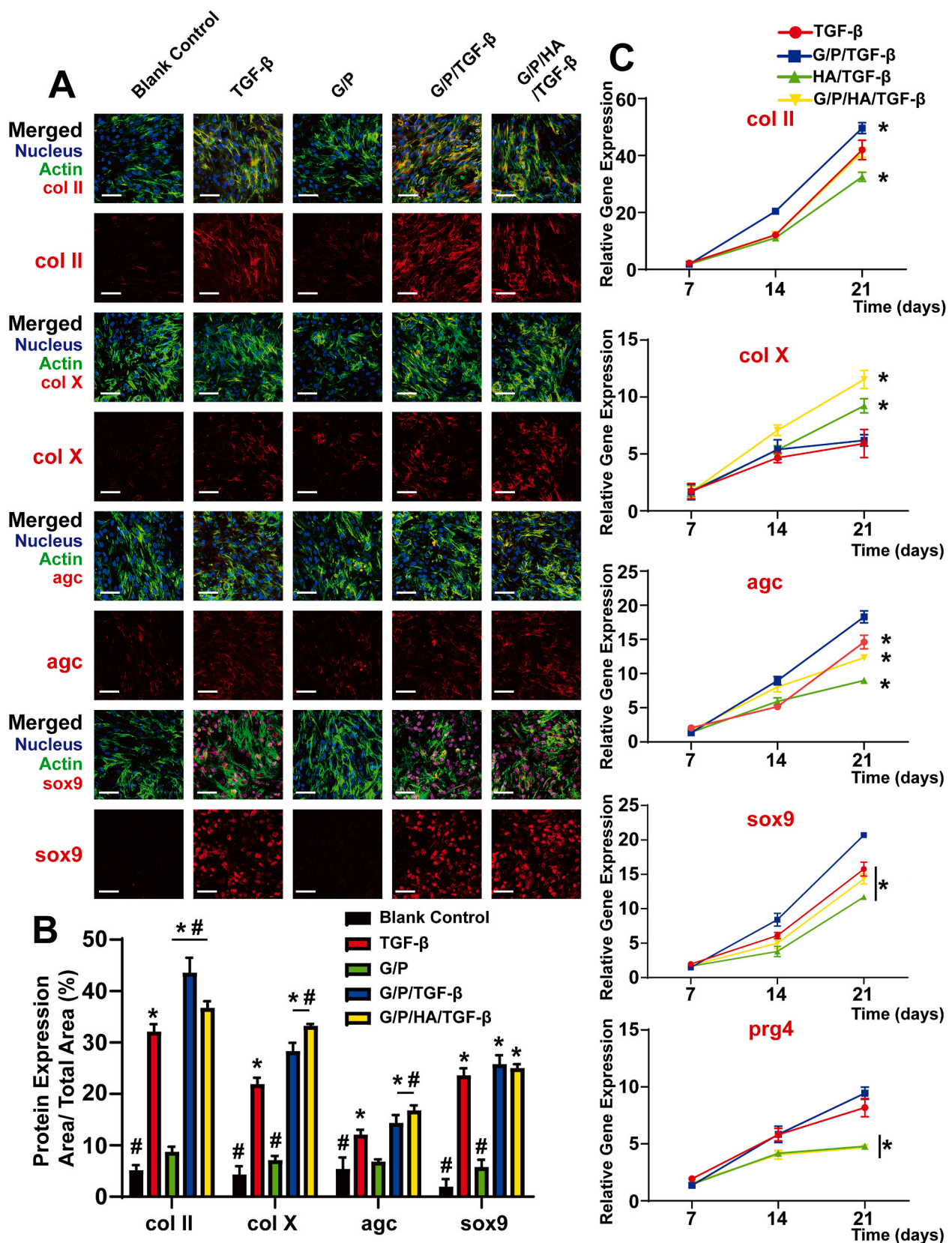
Fig. 5. Microspheres loaded with cytokines induce chondrogenesis differentiation and expression of specific proteins. A) Confocal images of BMSCs in the blank control, TGF-β, G/P, G/P/TGF-β, and G/P/HA/TGF-β detected via immunofluorescence labeling 21 days after cell seeding. Upper panels show "merged" (protein expression + nucleus + F-actin) staining and lower panels show protein expression. B) Quantitative evaluation of protein expression via ImageJ software. The results were expressed as protein expression area/total area × 100 (%). C) mRNA expression of col II, col X, agc, sox9, and prg4, as determined using qRT-PCR 21 days after cell seeding on the scaffold. Scale bar: 50 μm; *P < 0.05 compared with other groups. BMSC, bone marrow mesenchymal stem cell; G/P, gelatin/PLGA; HA, hydroxyapatite.
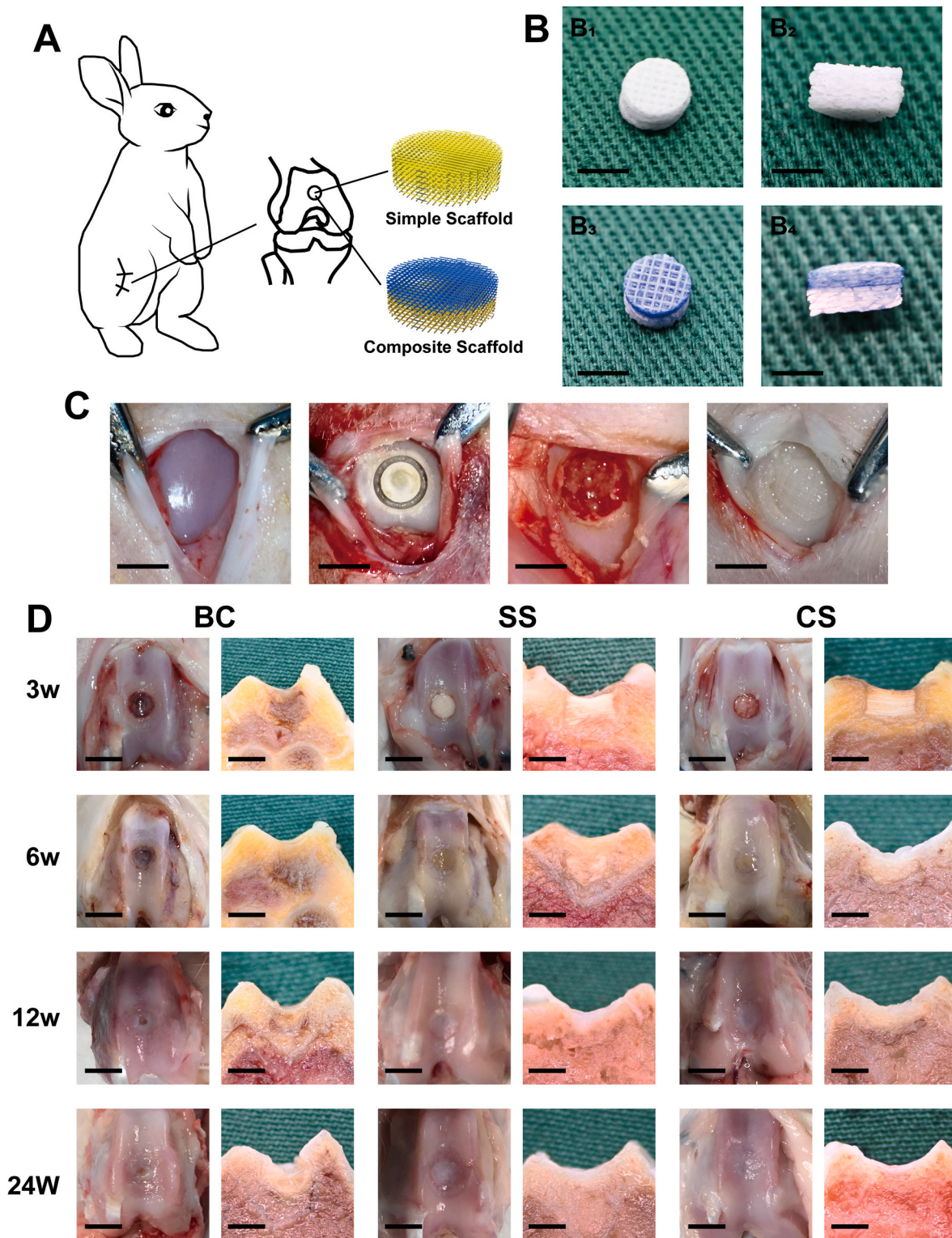
Fig. 6. Gross view and cross-sectional observation on the operation day and after harvesting. A) Schematic diagram of animal experiments. B) Gross view of the front and cross-section of the scaffold (B1 and B2), gross view and cross-section of the scaffold Inkjet using colored ink (B3 and B4). C) Gross view of surgical procedure; C) Gross view (left panel) and a cross-sectional view (right panel) of the blank control group, simple scaffold group, and composite scaffold group 3, 6, 12, and 24 weeks after scaffold implantation. Scale bar: 4 mm; BC, Blank Control; SS, Simple Scaffold; CS, Composite Scaffold.

formation, thereby promoting cartilage repair [35–37]. Combined with microfracture surgery to connect the bone marrow, we guided BMSCs to attach to the CS, thereby promoting cartilage repair.

Microfracture is one of the most common first-line minimally invasive surgeries and is widely used in the repair of intra-articular cartilage defects [15,38]. Penetrating the subchondral bone enables blood and bone marrow containing autologous BMSCs to easily flow to the cartilage defect site for tissue repair and regeneration. However, because of the regeneration of fibrocartilage, this method alone may not meet the clinical needs for repairing intra-articular cartilage defects. Therefore, in
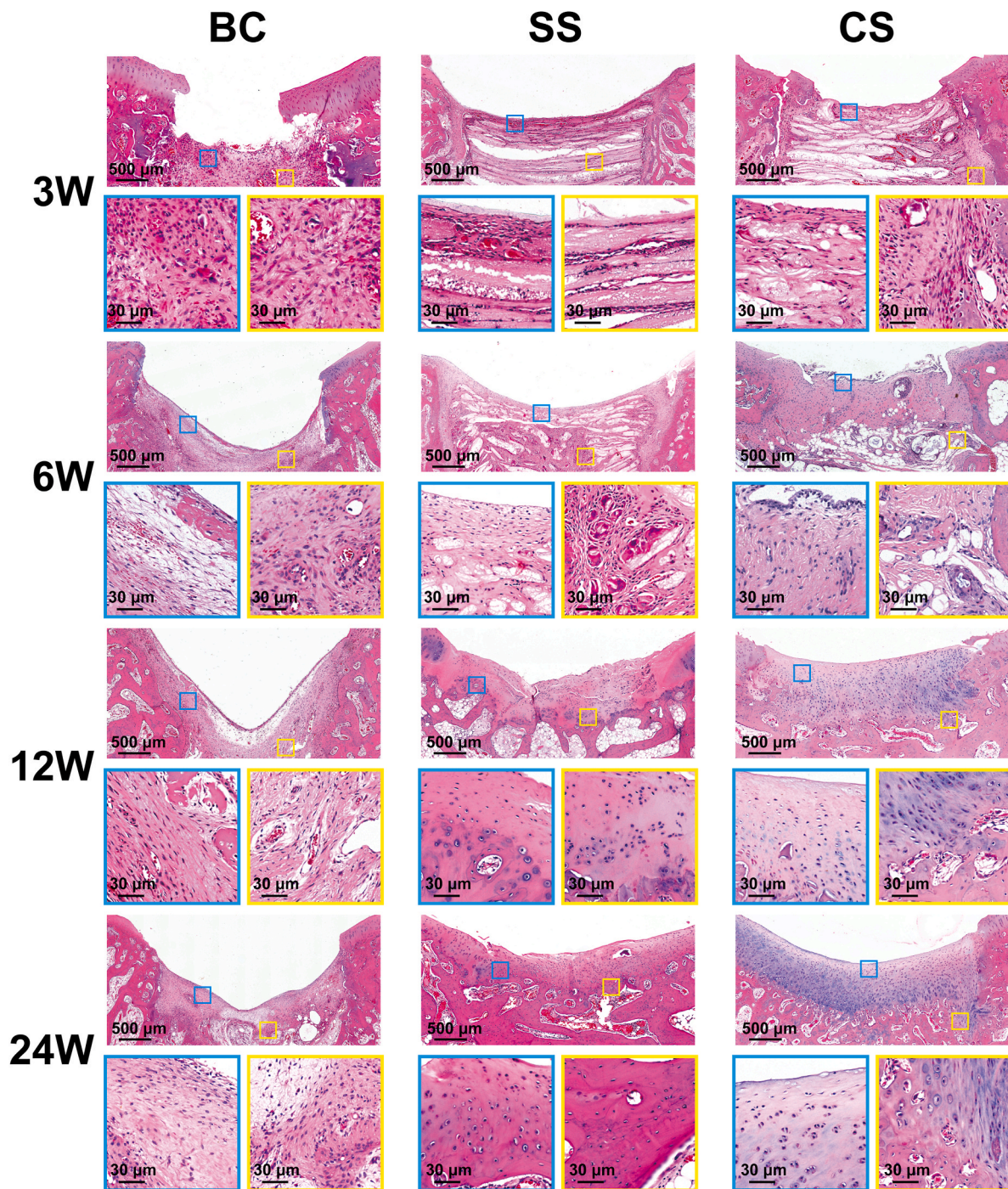
Fig. 7. Microscopic appearance of H&E-stained blank control, simple scaffold, and composite scaffold groups after 3, 6, 12 and 24 weeks. BC, Blank Control; SS, Simple Scaffold; CS, Composite Scaffold; H&E, hematoxylin and eosin.

this study, a CS with gelatin and PLGA was used as the basic material to support cell attachment and proliferation. This enabled the repair of the bone marrow blood clot via BMSCs. We then loaded TGF-β1 and HA in the scaffold to promote BMSCs differentiation into cartilage, thereby promoting cartilage repair [39–42].

To establish a good 3D structure and have layering characteristics, we combined MEW with Inkjet technology to construct a CS that could be loaded with specific cytokine-carrying microspheres at specific locations. MEW technology is a type of 3D printing technology [8,43–45]. Based on ordinary fused deposition modeling (FDM) 3D printing, by increasing the electric field, the ink passing through the needle base can be further pulled, thereby breaking the aperture limit of the printing

needle and achieving higher precision. In the past, electrospinning technology was used but was mostly used to prepare 2D electrospun nanofiber membranes [46–49]. When combined with 3D printing technology to obtain a 3D structure and achieve controlled printing, it is difficult for the wire diameter to reach the nanometer level of the nanofiber membrane, and the highest controllable precision can reach 1 μm [7,50]. For cartilage repair, the thickness of cartilage at the knee joint of humans is less than 3 mm. Therefore, compared to other extrusion printing methods, high-precision MEW is undoubtedly more in line with the requirements.

For MEW printing, the most commonly used material is PCL, which melts at approximately 65 °C and has good formability. However, the
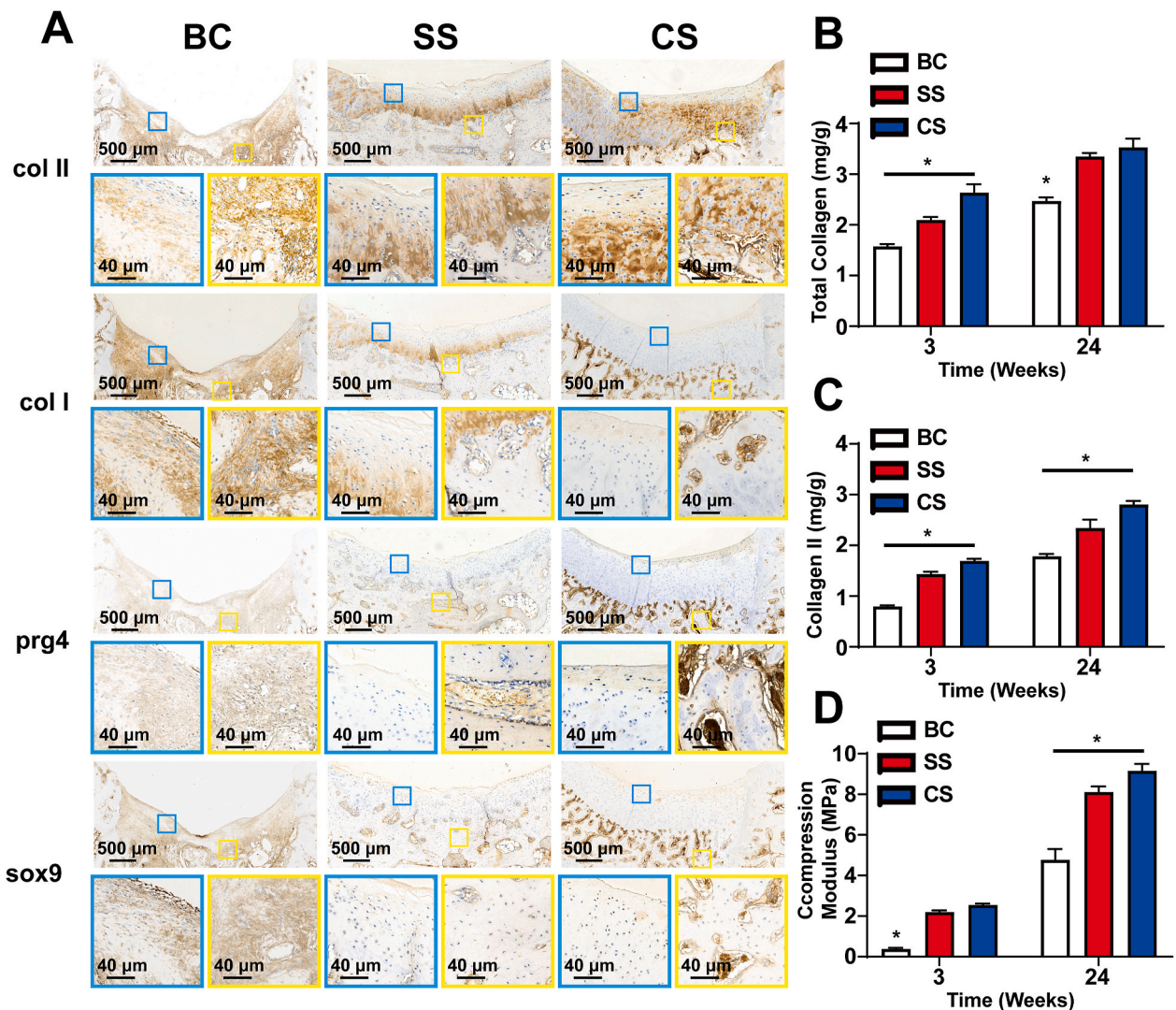
Fig. 8. Composition and mechanical analyses of regenerated cartilage. A) Immunohistochemical analysis of col II, col I, prg4, and sox9 expression levels in the regenerated cartilage of the blank control, simple scaffold and composite scaffold groups after 24 weeks; B) Total collagen content, C) col II content, and D) compression modulus of regenerated cartilage in various groups, as indicated, after 3 and 24 weeks. (*P < 0.05 compared to other groups; BC, Blank Control; SS, Simple Scaffold; CS, Composite Scaffold).

degradation rate of PCL is extremely slow, so there are still deficiencies in cartilage repair. Natural polymers, such as gelatin, have become a good source of bionic scaffolds for cartilage regeneration. Gelatin is a partial hydrolysate of collagen. It has good biocompatibility and biological activity and can promote collagen formation and cartilage repair. However, collagen is soluble in water and has a low viscosity after being dissolved in water or organic solvents; therefore, it is difficult to use it alone. It is mostly used by adding active groups to construct hydrogels or mixing with other materials [51–53].

PLGA, an FDA-approved polymer, is a copolymer of polylactic acid (PLA) and polyglycolide (PGA), which are widely used in tissue engineering. By adjusting the ratio of PLA to PGA in PLGA, the mechanical and degradation properties can be partially adjusted. The degradation cycle of PLGA (85:15) is about 3–5 months, which is closer to the time of cartilage repair. A longer explanation period is conducive to acidic metabolites of PLGA, reducing the possible impact [54,55].

In terms of solvents, hexafluoroisopropanol (HFIP) was chosen, which is safe and has a boiling point of approximately 59 °C, as well as good thermal stability. Gelatin and PLGA can form high-concentration solutions, and the viscosity increases with increasing solubility. Therefore, by adjusting the concentration of the solution, we could easily adjust the viscosity of the printer ink. During the printing process, the HFIP solution of G/P was placed in the barrel to form a partially sealed environment, which was not easy to volatilize and precipitate at room temperature. When extruding and printing on the receiving plate, the receiving plate was heated to 37 °C, which greatly accelerated the volatilization of HFIP without destroying the printing structure. In addition, the diameter of the filaments printed by MEW was small, about 10 μm, and a smaller diameter helped maintain the fiber shape. Compared with other printing methods, it had a larger surface area under the premise of the same amount of material, so it was better for the volatilization of HFIP. In this study, we increased the concentration of the solution, thereby increasing the viscosity and reducing the diameter of the printing filaments, so that the fiber could partially maintain the shape on the receiving plate. We also slightly increased the temperature of the receiving plate, increasing volatilization of the solution, so that support was established. However, the solubility of gelatin in HFIP was still limited; the highest was 15%, and a further increase in the concentration was difficult to achieve in 1 day, so we chose a concentration of 15%, and added PLGA to adjust the printing performance.

For MEW technology and even 3D printing technology, formability is

crucial. For MEW technology, the viscosity of the ink is essential. Ink with lower viscosity easily squeezes out and is easily pulled by the electric field, but it is difficult to control the flow rate, it easily collapses on the receiving plate, and it is not easy to pile up. ink with higher viscosity is not easy to release, and the electric field is not enough to pull it. Achieving a balance between the two is very important. We think that viscosity of 20–30 Pa s may be appropriate. In contrast, solidifying the fluid extruded in the barrel and the corresponding solidification time are also very important issues. Currently, the commonly used curing methods include cooling curing, light curing, chemical curing, and precipitation curing. In our research, we used precipitation curing to solidify the stent and shape it through solvent volatilization. The curing time should be as short as possible, especially to match the viscosity of the ink. The curing time should be quicker than when the solution fiber collapses. After clarifying these issues, MEW-based printing inks could be greatly expanded, and many current biological materials could be prepared and studied with higher precision.

Maintaining the microenvironment for BMSCs in the scaffold to form cartilage is also vital. TGF-β1 is a key regulator of BMSCs cartilage differentiation. TGF-β1 can be used as a cell culture supplement to promote cartilage formation in BMSCs and is recognized as the key to maintaining cartilage differentiation in vitro. Previous studies have also found that in surgically induced osteoarthritis or osteochondral defect models, TGF-β1 pretreatment of BMSCs had a good repair effect. Therefore, to promote better cartilage repair, we used PLGA microspheres to load TGF-β1 and performed Inkjet and MEW alternate printing, so that the microspheres were sprayed on the entire stent layer. This helped maintain the continuous effect of TGF-β1 and allowed the relevant proteins to be accurately placed on any part of the engineered scaffold, making it more flexible [26,56,57].

The lower part was mixed with HA nanoparticles in G/P. During cell adhesion on the scaffold, the cells could make contact with HA. The lower layer of cells was subjected to the combined effect of HA and TGF-β1, which promoted cell hypertrophy, and col x expression was higher, which could connect with the deep bone tissue. Khanarian et al. observed higher col x expression in prehypertrophic chondrocytes cultured with mixed HA from the deep layer of bovine articular cartilage [58]. Because the microfracture opens up the subchondral bone, the stent part communicates with the bone marrow, and the relative oxygen content in the deep layer is relatively high, which helps reduce the risk of hypoxia and promotes the expression of deep layer cartilage. The study by Steele et al. proved that hypoxia inhibits hypertrophy and endochondral ossification markers in the tibia explants of fetal mice [59]. In addition, Eslaminejad et al. reported that murine MSCs increased mineralization at a lower cell density in 2D cultures [60].

In this study, only Inkjet-printed TGF-β-loaded microspheres were used. However, in practical applications, various and more refined cytokine-loaded microspheres can be fabricated according to requirements. Here, to highlight the effect of using gelatin as a printing material, we simplified the layering effect. The printing accuracy of this system that used MEW and Inkjet was extremely high. we used a high-concentration G/P solution to prepare a high-viscosity ink suitable for MEW technology. We further explored the role of scaffolds in cartilage repair using this high-precision MEW and Inkjet technology to prepare a structural and functional biomimetic scaffold, construct a biologically active cartilage repair complex, verify the characteristics of the scaffold from the material and its biology, and study related biological activity and cytotoxicity. However, there are a few limitations to our research. Even if we improved the printing accuracy to the maximum extent possible, it cannot be compared with that of traditional PCL. In this regard, we will continue to study and further improve the technology.

5. Conclusion

This research demonstrates a novel printing ink based on fused MEW technology and its ability to repair cartilage. Through further exploration of MEW technology, this research clarified the conditions of ink moldability. The natural polymer material gelatin was mixed with PLGA to obtain a high-concentration and high-viscosity printing ink suitable for MEW, which was used to print a cartilage repair scaffold. At the same time, using Inkjet technology, cytokine-carrying microspheres were accurately loaded on the repair scaffold to construct a new high-precision cartilage repair scaffold with biological activity. In vitro, the CS has good biocompatibility and degradation properties that matched the cartilage repair speed. In vivo experiments showed that the scaffold can fill cartilage damage and promote repair of the damage. In general, this research provides a new printing system for bio-3D printing. The system has high precision and good biological activity and can provide new possibilities for the repair of cartilage damage.

CRediT authorship contribution statement

Yu Han: Conceptualization, Methodology, Writing – original draft, preparation. **Bo Jia:** Methodology, Investigation, Validation. **Meifei Lian:** Investigation, Formal analysis, Validation. **Binbin Sun:** Writing-Reviewing and Editing, Supervision. **Qiang Wu:** Investigation, Data curation. **Benlin Sun:** Formal analysis, Data curation. **Zhiguang Qiao:** Methodology, Investigation, Supervision. **Kerong Dai:** Writing-Reviewing and Editing, Supervision, Funding acquisition.

Declaration of competing interest

The authors have declared that no competing interests exist.

Appendix A. Supplementary data

Supplementary data related to this article can be found at https://doi.org/10.1016/j.bioactmat.2020.12.018.

References

[1] A.C. Daly, P. Pitacco, J. Nulty, G.M. Cunniffe, D.J. Kelly, 3D printed microchannel networks to direct vascularisation during endochondral bone repair, Biomaterials 162 (2018) 34–46.
[2] S.E. Majd, A.I. Rizqy, H.J. Kaper, T.A. Schmidt, R. Kuijer, P.K. Sharma, An in vitro study of cartilage-meniscus tribology to understand the changes caused by a meniscus implant, Colloids Surf. B Biointerfaces 155 (2017) 294–303.
[3] A.C. Daly, F.E. Freeman, T. Gonzalez-Fernandez, S.E. Critchley, J. Nulty, D.J. Kelly, 3D bioprinting for cartilage and osteochondral tissue engineering, Adv Healthc Mater 6 (22) (2017).
[4] A. Kosik-Kozioł, M. Costantini, T. Bolek, K. Szöke, A. Barbetta, J. Brinchmann, W. Święszkowski, PLA short sub-micron fiber reinforcement of 3D bioprinted alginate constructs for cartilage regeneration, Biofabrication 9 (4) (2017).
[5] S.M. McNary, K.A. Athanasiou, A.H. Reddi, Engineering lubrication in articular cartilage, Tissue Eng. B Rev. 18 (2) (2012) 88–100.
[6] A.C. Daly, S.E. Critchley, E.M. Rencsok, D.J. Kelly, A comparison of different bioinks for 3D bioprinting of fibrocartilage and hyaline cartilage, Biofabrication 8 (4) (2016), 045002.
[7] A. Hrynevich, B.S. Elci, J.N. Haigh, R. McMaster, A. Youssef, C. Blum, T. Blunk, G. Hochleitner, J. Groll, P.D. Dalton, Dimension-based design of melt electrowritten scaffolds, Small 14 (22) (2018), e1800232.

[8] G. Hochleitner, F. Chen, C. Blum, P.D. Dalton, B. Amsden, J. Groll, Melt electrowriting below the critical translation speed to fabricate crimped elastomer scaffolds with non-linear extension behaviour mimicking that of ligaments and tendons, Acta Biomater. 72 (2018) 110–120.

[9] J.B. Choi, I. Youn, L. Cao, H.A. Leddy, C.L. Gilchrist, L.A. Setton, F. Guilak, Zonal changes in the three-dimensional morphology of the chondron under compression: the relationship among cellular, pericellular, and extracellular deformation in articular cartilage, J. Biomech. 40 (12) (2007) 2596–2603.

[10] M.E. Cooke, A.A. Allon, T. Cheng, A.C. Kuo, H.T. Kim, T.P. Vail, R.S. Marcucio, R. A. Schneider, J.C. Lotz, T. Alliston, Structured three-dimensional co-culture of mesenchymal stem cells with chondrocytes promotes chondrogenic differentiation without hypertrophy, Osteoarthritis Cartilage 19 (10) (2011) 1210–1218.

[11] Z.M. Liu, P.C. Shen, C.C. Lu, S.H. Chou, Y.C. Tien, Characterization of the Proliferating Layer Chondrocytes of Growth Plate for Cartilage Regeneration, Tissue Eng Part A, 2018.

[12] C. Wang, W. Huang, Y. Zhou, L. He, Z. He, Z. Chen, X. He, S. Tian, J. Liao, B. Lu, Y. Wei, M. Wang, 3D printing of bone tissue engineering scaffolds, Bioact Mater 5 (1) (2020) 82–91.

[13] L. Wei, S. Wu, M. Kuss, X. Jiang, R. Sun, P. Reid, X. Qin, B. Duan, 3D printing of silk fibroin-based hybrid scaffold treated with platelet rich plasma for bone tissue engineering, Bioact Mater 4 (2019) 256–260.

[14] H. Kang, Y. Zeng, S. Varghese, Functionally graded multilayer scaffolds for in vivo osteochondral tissue engineering, Acta Biomater. 78 (2018) 365–377.

[15] T. Guo, M. Noshin, H.B. Baker, E. Taskoy, S.J. Meredith, Q. Tang, J.P. Ringel, M. J. Lerman, Y. Chen, J.D. Packer, J.P. Fisher, 3D printed biofunctionalized scaffolds for microfracture repair of cartilage defects, Biomaterials 185 (2018) 219–231.

[16] L. Ruiz-Cantu, A. Gleadall, C. Faris, J. Segal, K. Shakesheff, J. Yang, Multi-material 3D bioprinting of porous constructs for cartilage regeneration, Mater Sci Eng C Mater Biol Appl 109 (2020) 110578.

[17] S. Stratton, N.B. Shelke, K. Hoshino, S. Rudraiah, S.G. Kumbar, Bioactive polymeric scaffolds for tissue engineering, Bioact Mater 1 (2) (2016) 93–108.

[18] J.W. Nichol, S.T. Koshy, H. Bae, C.M. Hwang, S. Yamanlar, A. Khademhosseini, Cell-laden microengineered gelatin methacrylate hydrogels, Biomaterials 31 (21) (2010) 5536–5544.

[19] K.Y. Lee, D.J. Mooney, Hydrogels for tissue engineering, Chem. Rev. 101 (7) (2001) 1869–1879.

[20] D. Loessner, C. Meinert, E. Kaemmerer, L.C. Martine, K. Yue, P.A. Levett, T.J. Klein, F.P. Melchels, A. Khademhosseini, D.W. Hutmacher, Functionalization, preparation and use of cell-laden gelatin methacryloyl-based hydrogels as modular tissue culture platforms, Nat. Protoc. 11 (4) (2016) 727–746.

[21] K. Dey, S. Agnelli, L. Sartore, Dynamic freedom: substrate stress relaxation stimulates cell responses, Biomater Sci 7 (3) (2019) 836–842.

[22] X.S. Wu, N. Wang, Synthesis, characterization, biodegradation, and drug delivery application of biodegradable lactic/glycolic acid polymers. Part II: biodegradation, J. Biomater. Sci. Polym. Ed. 12 (1) (2001) 21–34.

[23] P. Davoudi, S. Assadpour, M.A. Derakhshan, J. Ai, A. Solouk, H. Ghanbari, Biomimetic modification of polyurethane-based nanofibrous vascular grafts: a promising approach towards stable endothelial lining, Mater Sci Eng C Mater Biol Appl 80 (2017) 213–221.

[24] S. Moeinzadeh, S.R. Pajoum Shariati, E. Jabbari, Comparative effect of physicomechanical and biomolecular cues on zone-specific chondrogenic differentiation of mesenchymal stem cells, Biomaterials 92 (2016) 57–70.

[25] J. Ma, Y. He, X. Liu, W. Chen, A. Wang, C.Y. Lin, X. Mo, X. Ye, A novel electrospun-aligned nanoyarn/three-dimensional porous nanofibrous hybrid scaffold for annulus fibrosus tissue engineering, Int. J. Nanomed. 13 (2018) 1553–1567.

[26] T. Re'em, Y. Kaminer-Israeli, E. Ruvinov, S. Cohen, Chondrogenesis of hMSC in affinity-bound TGF-beta scaffolds, Biomaterials 33 (3) (2012) 751–761.

[27] X. Ji, Z. Lei, M. Yuan, H. Zhu, X. Yuan, W. Liu, H. Pu, J. Jiang, Y. Zhang, X. Jiang, J. Xiao, Cartilage repair mediated by thermosensitive photocrosslinkable TGFbeta1-loaded GM-HPCH via immunomodulating macrophages, recruiting MSCs and promoting chondrogenesis, Theranostics 10 (6) (2020) 2872–2887.

[28] N.J. Castro, J. O'Brien, L.G. Zhang, Integrating biologically inspired nanomaterials and table-top stereolithography for 3D printed biomimetic osteochondral scaffolds, Nanoscale 7 (33) (2015) 14010–14022.

[29] I. Khan, R. Nagarjuna, J.R. Dutta, R. Ganesan, Enzyme-embedded degradation of poly(epsilon-caprolactone) using lipase-derived from probiotic lactobacillus plantarum, ACS Omega 4 (2) (2019) 2844–2852.

[30] A. He, H. Xia, K. Xiao, T. Wang, Y. Liu, J. Xue, D. Li, S. Tang, F. Liu, X. Wang, W. Zhang, W. Liu, Y. Cao, G. Zhou, Cell yield, chondrogenic potential, and regenerated cartilage type of chondrocytes derived from ear, nasoseptal, and costal cartilage, J Tissue Eng Regen Med 12 (4) (2018) 1123–1132.

[31] A. He, L. Liu, X. Luo, Y. Liu, Y. Liu, F. Liu, X. Wang, Z. Zhang, W. Zhang, W. Liu, Y. Cao, G. Zhou, Repair of osteochondral defects with in vitro engineered cartilage based on autologous bone marrow stromal cells in a swine model, Sci. Rep. 7 (2017) 40489.

[32] E. Ruvinov, T. Tavor Re'em, F. Witte, S. Cohen, Articular cartilage regeneration using acellular bioactive affinity-binding alginate hydrogel: a 6-month study in a mini-pig model of osteochondral defects, J Orthop Translat 16 (2019) 40–52.

[33] T. Sueyoshi, K. Yamamoto, H. Akiyama, Conditional deletion of Tgfbr2 in hypertrophic chondrocytes delays terminal chondrocyte differentiation, Matrix Biol. 31 (6) (2012) 352–359.

[34] J.A. Andrades, S.C. Motaung, P. Jimenez-Palomo, S. Claros, J.M. Lopez-Puerta, J. Becerra, T.M. Schmid, A.H. Reddi, Induction of superficial zone protein (SZP)/

[lubricin/PRG 4 in muscle-derived mesenchymal stem/progenitor cells by transforming growth factor-beta 1 and bone morphogenetic protein-7, Arthritis Res. Ther. 14 (2) (2012) R72.

[35] M. Bhattacharjee, J. Coburn, M. Centola, S. Murab, A. Barbero, D.L. Kaplan, I. Martin, S. Ghosh, Tissue engineering strategies to study cartilage development, degeneration and regeneration, Adv. Drug Deliv. Rev. 84 (2015) 107–122.

[36] T. Guo, J. Lembong, L.G. Zhang, J.P. Fisher, Three-dimensional printing articular cartilage: recapitulating the complexity of native Tissue<sup/>, Tissue Eng. B Rev. 23 (3) (2017) 225–236.

[37] H.W. Kang, S.J. Lee, I.K. Ko, C. Kengla, J.J. Yoo, A. Atala, A 3D bioprinting system to produce human-scale tissue constructs with structural integrity, Nat. Biotechnol. 34 (3) (2016) 312–319.

[38] M.S. Kim, C.H. Chun, J.H. Wang, J.G. Kim, S.B. Kang, J.D. Yoo, J.G. Chon, M. K. Kim, C.W. Moon, C.B. Chang, I.S. Song, J.K. Ha, N.Y. Choi, Y. In, Microfractures versus a Porcine-Derived Collagen-Augmented Chondrogenesis Technique for Treating Knee Cartilage Defects: A Multicenter Randomized Controlled Trial, Arthroscopy, 2019.

[39] N.S. Kalson, P.D. Gikas, T.W. Briggs, Current strategies for knee cartilage repair, Int. J. Clin. Pract. 64 (10) (2010) 1444–1452.

[40] Y. Nam, Y.A. Rim, J. Lee, J.H. Ju, Current therapeutic strategies for stem cell-based cartilage regeneration, Stem Cell. Int. 2018 (2018), 8490489.

[41] G. Musumeci, C. Loreto, S. Castorina, R. Imbesi, R. Leonardi, P. Castrogiovanni, Current concepts in the treatment of cartilage damage. A review, Ital. J. Anat Embryol. 118 (2) (2013) 189–203.

[42] M. Cully, Regenerative medicine: adhesive-hydrogel composite developed to repair damaged cartilage, Nat. Rev. Rheumatol. 9 (3) (2013) 135.

[43] M.L. Jorgensen, C. Muller, M. Sikkersoq, M. Nadzieja, Z. Zhang, Y. Su, J. Just, K. L. Garm Spindler, M. Chen, A melt-electrowritten filter for capture and culture of circulating colon cancer cells, Mater Today Bio 6 (2020) 100052.

[44] E. Hewitt, S. Mros, M. McConnell, J.D. Cabral, A. Ali, Melt-electrowriting with novel milk protein/PCL biomaterials for skin regeneration, Biomed. Mater. 14 (5) (2019), 055013.

[45] G. Hochleitner, E. Fursattel, R. Giesa, J. Groll, H.W. Schmidt, P.D. Dalton, Melt electrowriting of thermoplastic elastomers, Macromol. Rapid Commun. 39 (10) (2018), e1800055.

[46] K. Ye, K. Kuang, Z. You, Y. Morsi, X. Mo, Electrospun nanofibers for tissue engineering with drug loading and release, Pharmaceutics 11 (4) (2019).

[47] M.R. Casanova, M. Alves da Silva, A.R. Costa-Pinto, R.L. Reis, A. Martins, N. M. Neves, Chondrogenesis-inductive nanofibrous substrate using both biological fluids and mesenchymal stem cells from an autologous source, Mater Sci Eng C Mater Biol Appl 98 (2019) 1169–1178.

[48] W. Su, Z. Wang, J. Jiang, X. Liu, J. Zhao, Z. Zhang, Promoting tendon to bone integration using graphene oxide-doped electrospun poly(lactic-co-glycolic acid) nanofibrous membrane, Int. J. Nanomed. 14 (2019) 1835–1847.

[49] Y. Chen, M. Shafiq, M. Liu, Y. Morsi, X. Mo, Advanced fabrication for electrospun three-dimensional nanofiber aerogels and scaffolds, Bioact Mater 5 (4) (2020) 963–979.

[50] N.T. Saidy, F. Wolf, O. Bas, H. Keijdener, D.W. Hutmacher, P. Mela, E.M. De-Juan-Pardo, Biologically inspired scaffolds for heart valve tissue engineering via melt electrowriting, Small 15 (24) (2019), e1900873.

[51] J.H. Galarraga, M.Y. Kwon, J.A. Burdick, 3D bioprinting via an in situ crosslinking technique towards engineering cartilage tissue, Sci. Rep. 9 (1) (2019) 19987.

[52] D. Dranseikiene, S. Schrufer, D.W. Schubert, S. Reakasame, A.R. Boccaccini, Cell-laden alginate dialdehyde-gelatin hydrogels formed in 3D printed sacrificial gel, J. Mater. Sci. Mater. Med. 31 (3) (2020) 31.

[53] A.L.Y. Nachlas, S. Li, B.W. Streeter, K.J. De Jesus Morales, F. Sulejmani, D. I. Madukauwa-David, D. Bejleri, W. Sun, A.P. Yoganathan, M.E. Davis, A multilayered valve leaflet promotes cell-laden collagen type I production and aortic valve hemodynamics, Biomaterials 240 (2020) 119838.

[54] N.T. Hiep, B.T. Lee, Electro-spinning of PLGA/PCL blends for tissue engineering and their biocompatibility, J. Mater. Sci. Mater. Med. 21 (6) (2010) 1969–1978.

[55] M. Chen, S. Jiang, F. Zhang, L. Li, H. Hu, H. Wang, Graphene oxide immobilized PLGA-polydopamine nanofibrous scaffolds for growth inhibition of colon cancer cells, Macromol. Biosci. 18 (12) (2018), e1800321.

[56] C.Y. Lin, Y.H. Chang, K.C. Li, C.H. Lu, L.Y. Sung, C.L. Yeh, K.J. Lin, S.F. Huang, T. C. Yen, Y.C. Hu, The use of ASCs engineered to express BMP2 or TGF-beta 3 within scaffold constructs to promote calvarial bone repair, Biomaterials 34 (37) (2013) 9401–9412.

[57] W. Wang, B. Li, Y. Li, Y. Jiang, H. Ouyang, C. Gao, In vivo restoration of full-thickness cartilage defects by poly(lactide-co-glycolide) sponges filled with fibrin gel, bone marrow mesenchymal stem cells and DNA complexes, Biomaterials 31 (23) (2010) 5953–5965.

[58] N.T. Khanarian, N.M. Haney, R.A. Burga, H.H. Lu, A functional agarose-hydroxyapatite scaffold for osteochondral interface regeneration, Biomaterials 33 (21) (2012) 5247–5258.

[59] J.A. Steele, S.D. McCullen, A. Callanan, H. Autefage, M.A. Accardi, D. Dini, M. M. Stevens, Combinatorial scaffold morphologies for zonal articular cartilage engineering, Acta Biomater. 10 (5) (2014) 2065–2075.

[60] M.B. Eslaminejad, S. Nadri, Murine mesenchymal stem cell isolated and expanded in low and high density culture system: surface antigen expression and osteogenic culture mineralization, In Vitro Cell. Dev. Biol. Anim. 45 (8) (2009) 451–459.